Phase formation and texture development in mullite/zirconia composites fabricated by templated grain growth

C. DURAN*, Y. K. TÜR
Department of Materials Science and Engineering, Gebze Institute of Technology, P. K. 141, 41400, Gebze-Kocaeli, Turkey
E-mail: cduran@gyte.edu.tr

Published online: 12 April 2006

Mullite is a promising candidate for advanced ceramic applications but its low fracture toughness and difficulties in sintering are the main limitations for more widespread industrial applications. Therefore, mullite/zirconia composites were prepared from a reactive mixture of alumina and zircon powders. Additives, TiO_2 and MgO, were used to modify aluminosilicate glass to increase densification and <001> aluminum borate templates were incorporated to texture mullite in [001] by templated grain growth. Mullite/zirconia phase formation was complete at 1450°C in the presence of both templates and additives, as compared to 1500°C for the samples with only additives and to 1600°C for the samples with only templates. Dense mullite/zirconia composites with highly <001>-textured mullite grains (Lotgering factor ∼1) and a retention of ∼13% tetragonal ZrO_2 were fabricated after sintering at 1450°C for 2 h. A high quality of mullite texture with a degree of orientation parameter of 0.22 and a narrow distribution of elongated mullite grains within 8.8° around [001] were successfully obtained in the composites.

1. Introduction

Mullite is a promising candidate for advanced ceramic applications due to its low density, low thermal conductivity, low dielectric constant, low thermal expansion, excellent creep resistance and high temperature strength [1–4]. However, low fracture toughness and difficulties in sintering to attain full densification are the main limitations for mullite materials for more widespread engineering applications in industry [5]. One method to improve the mechanical properties of mullite is to employ mullite/zirconia ($3Al_2O_3{\cdot}2SiO_2/ZrO_2$) composites. It has been reported that significant toughening can be obtained by addition of zirconia particles to a mullite matrix [5–10]. Another method utilized to induce anisotropic mechanical properties is templated grain growth (TGG) [11]. It is a technique to develop crystallographic texture in polycrystalline ceramic bodies via the grain growth of aligned template particles. TGG relies on the use of anisotropically-shaped (i.e. whisker or platelet) single crystal templates because they can be oriented by shear forming processes such as tape casting and extrusion. The presence of a liquid is necessary for growth to occur [12]. Reaction sintering of alumina (Al_2O_3) and zircon ($ZrSiO_4$) is a simple and inexpensive route to fabricate mullite/zirconia composites with improved mechanical properties. In literature, kinetics of phase formation, microstructure evolution, effect of additives, and type of starting powders have been extensively studied by many researchers [6, 8–10, 13–17].

Chemical and thermal stability of templates as well as epitaxial relationship between the template and polycrystalline matrix are among the main requirements of the TGG process [12]. Aluminum borate ($9Al_2O_3{\cdot}2B_2O_3$) has a similar crystallographic structure to mullite [18, 19] and was successfully shown to behave as heteroepitaxial nucleation sites for enhanced mullite transformation kinetics [20]. Gonenli and Messing [21] found that when the aluminum borate whiskers were heated by themselves in air, they were transformed to α-Al_2O_3 at $T > 1400$°C. However, the templates were found to be stable enough to induce ⟨001⟩-mullite grain growth in a TiO_2-doped mullite even after heat treatment at 1500°C [21].

In earlier TGG mullite studies, acicular aluminum borate [21] and mullite [22] templates were used to fabricate highly textured mullite in [001]. In addition, randomly-

*Author to whom all correspondence should be addressed.
0022-2461
DOI: 10.1007/s10853-005-5454-2

oriented templates dispersed in the mullite matrix (e.g., β-Si_3N_4- or mullite-whisker/mullite matrix [23], Al_2O_3- or SiC-platelet/mullite matrix [24]) were used as second phase reinforcing agents, rather than texturing purpose.

In this study, <001>-oriented aluminum borate whiskers were used to texture mullite in [001] in the final mullite/zirconia composites without and with the additives of TiO_2 and MgO. It is aimed to induce multiple toughening mechanisms simultaneously from both textured mullite grains (by crack deflection, crack bowing, crack bridging and whisker pullout mechanisms) and tetragonal ZrO_2 grains (by transformation toughening and microcracking mechanisms) dispersed among the textured mullite grains to increase the fracture toughness of the composites. By this way, both elongated mullite grains and dispersed ZrO_2 grains will be effective together in the property increment. In this part of study, densification, mullite/zirconia phase formation from a reactive mixture of Al_2O_3 and $ZrSiO_4$, and texture evolution and characterization will be reported.

2. Experimental procedure

Mullite/zirconia composites were prepared by reactive sintering of α-Al_2O_3 (Alcoa, SG3000) and $ZrSiO_4$ (Eczacıbaşı, Doğa) powders. As-received aluminum borate ($9Al_2O_3{\cdot}2B_2O_3$) whiskers (Shikoku Chemical Co.) were used as templates to texture mullite in [001] in the composites. TiO_2 (Merck, Rutile type) and MgO (Merck) were added both to accelerate mullite/zirconia phase formation and to promote anisotropic grain growth of mullite during sintering. The mean particle sizes of 0.32 μm for Al_2O_3, 0.71 μm for $ZrSiO_4$, 0.12 μm for TiO_2, and 3.26 μm for MgO were measured using a laser particle size analyzer (Mastersizer 2000, Malvern Instruments Ltd.) after each powder was separately dispersed in water by ball milling for 24 h, using ammonium salt of poly(acrylic acid) (PAA-NH_4) (Darvan 821A, R. T. Vanderbilt Company, Inc.).

Table I summarizes sample designation, template concentration and additive contents in the composites. The samples prepared are MZ-TMA and MZ-A for template-containing batches and MZ-TM for a template-free batch. In the nomenclature, MZ refers to stoichiometric mullite/zirconia, T to TiO_2, M to MgO and A to the aluminum borate templates. For MZ-TMA and MZ-TM, the matrix is consisted of 3.4 wt% TiO_2 and 1.2 wt.% MgO in addition to Al_2O_3 and $ZrSiO_4$. Note that a template content of 10 wt.% was calculated with respect to the total amount of powders present in the MZ-TMA and MZ-A. Besides, Al_2O_3 from aluminum borate was not compensated by adding excess SiO_2 to the matrix powder.

TABLE I Sample designation, template and additive contents in the mullite/zirconia composites

Sample code	Additive content, wt% (vol%)		Template content, wt% (vol%)
	TiO_2	MgO	
MZ-TMA	3.4 (3.4)	1.2 (1.5)	10 (15.2)
MZ-TM	3.4 (3.4)	1.2 (1.5)	–
MZ-A	–	–	10 (15.2)

Samples were prepared by tape casting appropriate amounts of ceramic powders, using PAA-NH_4 as a dispersant, polyvinyl alcohol (PVA) (Sigma) as a binder and glycerol (Aldrich) as a plasticizer. Several drops of ethylene glycol surfactant (Surfynol 104E, Air Products) were added to remove air bubbles formed during slurry preparation. Tape casting was performed on a glass substrate at a casting speed of ~10 cm/s and a blade gap of 200 μm. Green tapes were cut and laminated at room temperature. Polymer burnout was carried out at 350°C. Details of aqueous tape casting and green sample preparation were described in our earlier study [25]. Samples were sintered between 1100 and 1600°C for 2 h with a constant heating rate of 7°C/min in air. The density of the samples was determined using the Archimedes technique.

Fig. 1 depicts the schematic view of samples used for the characterization. Parallel samples (hereafter denoted as "//") were sintered, then polished to 3 μm using diamond paste and, finally, thermally etched at 50°C below the sintering temperature for 30 min in air. Perpendicular-cut samples (hereafter denoted as "⊥"), however, were sliced from textured pieces and polished to yield flat surfaces.

Morphological texture was characterized on the // samples, using a scanning electron microscopy (SEM) (Philips XL30 SFEG). Crystallographic texture and orientation distribution were calculated from the ⊥-cut samples, using X-ray diffraction (XRD) (Rigaku Dmax 2200). The amount of texture, f, for mullite was calculated from Lotgering factor [26],

$$f = (P - P^{\circ})/(1 - P^{\circ}) \quad (1)$$

where P and P° are $[I_{(001)} + I_{(002)}]/\sum I_{(hkl)}$ in the textured and random mullite, respectively. The orientation distribution was obtained from rocking-curves [27], using the (002) mullite peak. The rocking curves were corrected for background, absorption, and defocus using Texture-Plus software [28]. The orientation distribution was calculated by fitting the corrected rocking curves to the March-Dollase equation [29, 30]:

$$P(f, r, \alpha) = f(r^2 \cos^2 \alpha + r^{-1} \sin^2 \alpha)^{-3/2} + (1 - f) \quad (2)$$

where f is the texture fraction, r is the degree of orientation parameter, and α is the misalignment angle from the texture direction (e.g., [001]). The r parameter is 1 for random and 0 for perfectly textured materials.

3. Results and discussion

3.1. Phase formation

Figs 2 and 3 show the XRD patterns obtained from the ⊥-cut MZ-TMA and ⊥-cut MZ-A samples, respec-

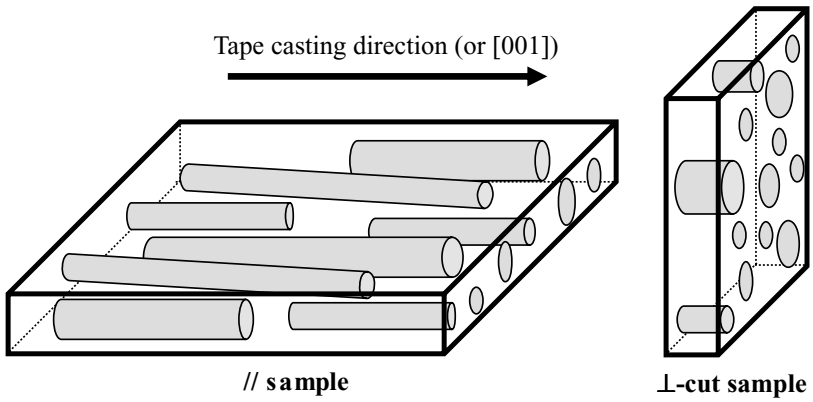

Figure 1 Schematic view of samples used for characterization.

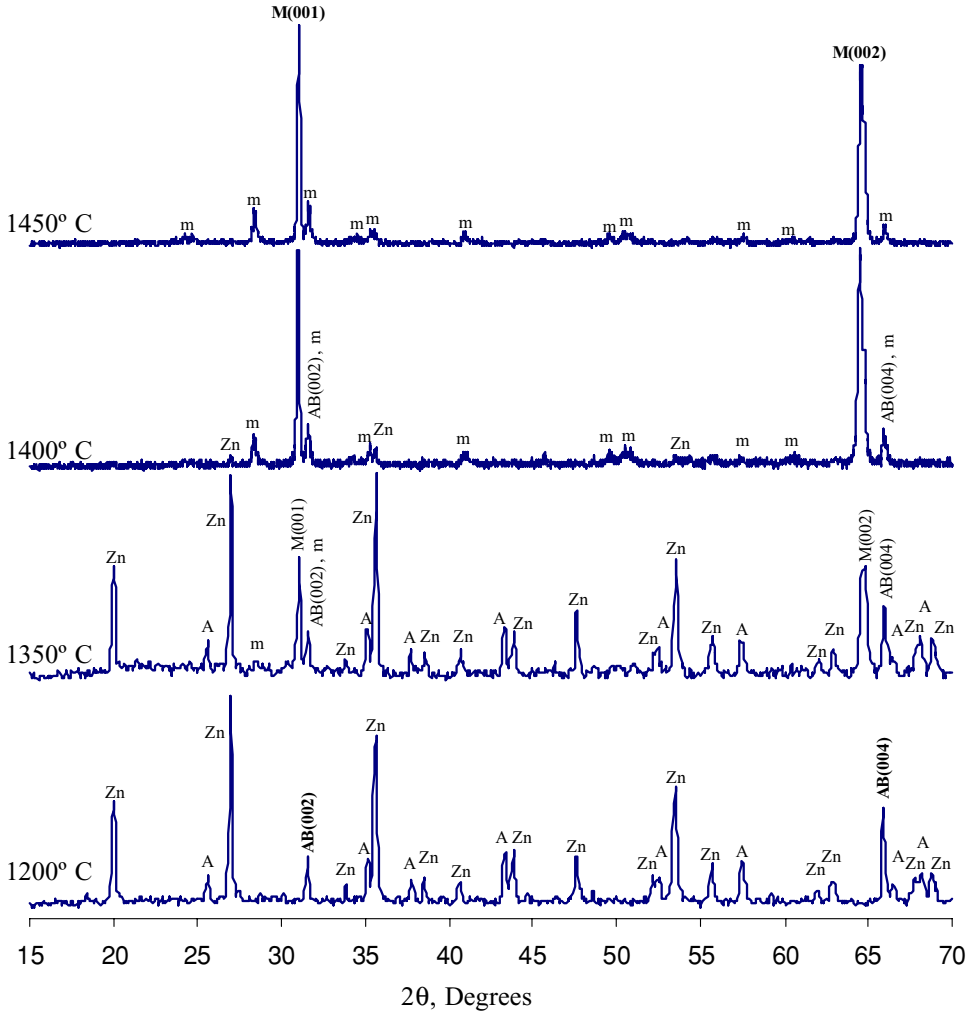

Figure 2 XRD patterns of the ⊥-cut MZ-TMA samples after sintering for 2 h. A: Alumina, Zn: Zircon, M: Mullite, AB: Aluminum borate, m: monoclinic zirconia.

tively. Major peaks are marked on the patterns. Fig. 2 shows in MZ-TMA that zircon was mainly consumed between 1350°C and 1400°C. Alumina was last detected at 1350°C. In MZ-A (Fig. 3), however, zircon decomposition happened gradually in a broad and at higher temperature range, that is, between 1450°C and 1550°C. Alumina was also detected at 1550°C. Samples with additives and no templates (MZ-TM) had reaction sequences in between MZ-TMA and MZ-A.

The extent of mullite formation (β) as a function of composition and temperature was calculated from XRD peak height intensities and is given in Fig. 4. For this analysis, mullite (001) at $2\theta = 30.96^{\circ}$ (JCPDS # 15-0776) for the textured samples (MZ-TMA and MZ-A) and mullite

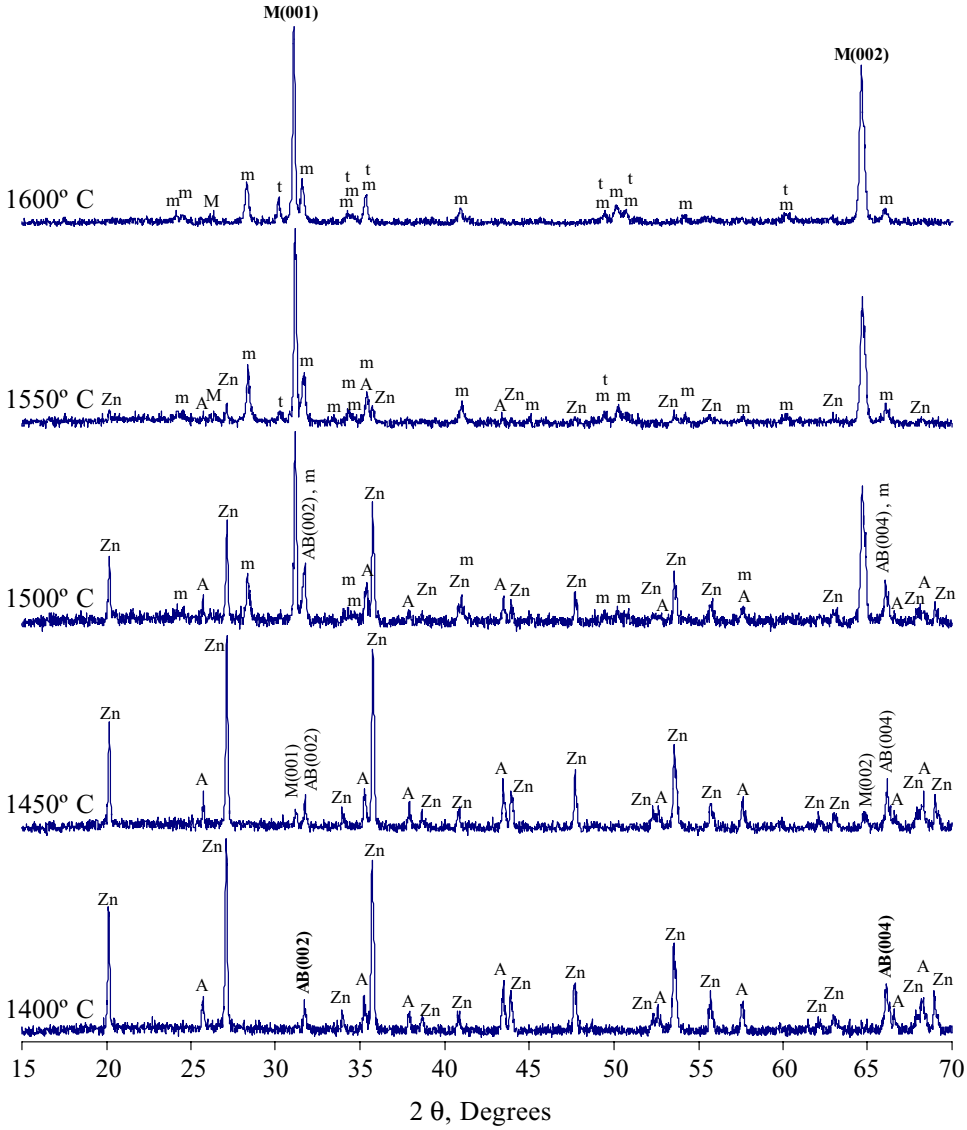

Figure 3 XRD patterns of the ⊥-cut MZ-A samples after sintering for 2 h. A: Alumina, Zn: Zircon, M: Mullite, AB: Aluminum borate, m: monoclinic zirconia, t: tetragonal zirconia.

(210) at $2\theta = 26.26^\circ$ for the random samples (MZ-TM) were used. β was then calculated as the ratio of mullite to mullite + Al_2O_3 (113) at $2\theta = 43.36^\circ$ (JCPDS # 10-0173). Fig. 4 shows that mullite formation was complete at 1400°C in MZ-TMA, 1500°C in MZ-TM and 1600°C in MZ-A. In addition, fully-formed mullite/zirconia composites were obtained at 1450°C in MZ-TMA (Fig. 2), 1500°C in MZ-TM and 1600°C in MZ-A (Fig. 3). Mullite and ZrO_2 formations were found to take place parallel to each other with temperature in MZ-TM and MZ-A. In MZ-TMA, however, no Al_2O_3 peaks are observed at 1400°C although weak zircon peaks are still present (as seen in Fig. 2), indicating that mullite formation was complete at relatively lower temperature than that for ZrO_2 evolution (1400°C vs. 1450°C). Absence of the Al_2O_3 peaks may be due to the fact that Al_2O_3 amount might be too low to be detected by XRD because zircon dissociation and Al_2O_3 consumption to form mullite are very fast between 1350°C and 1400°C (see Figs 2 and 4). XRD studies further showed that crystalline SiO_2 peaks (e.g., cristobalite) were not observed in any of the samples, which indicates that SiO_2 remained amorphous during the reactions. Also, no evidence of recrystallization of aluminum titanate, spinel and magnesium silicates took place during mullite/ZrO_2 formation, as determined by XRD.

Mullite formation from various reactive or coated powders or precursors was reported to originate from a transitory amorphous aluminosilicate phase [17, 31, 32]. Zhao *et al*. [33] postulated based on TEM analysis that mullite formation in the $ZrSiO_4/Al_2O_3$ system follows the nucleation and growth mechanism within the amorphous matrix. Mullite/zirconia composite formation from a reactive mixture of alumina and zircon is expressed as follows;

$$3Al_2O_3 + 2ZrSiO_4 \rightarrow 3Al_2O_3 \cdot 2SiO_2 + 2ZrO_2 \quad (3)$$

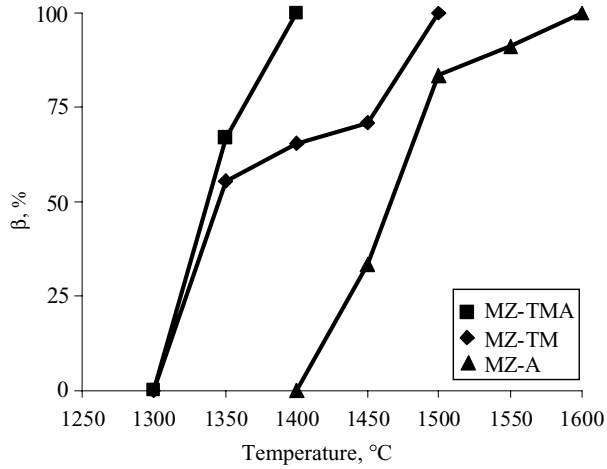

Figure 4 Phase formation of mullite (β) as a function of composition and sintering temperature.

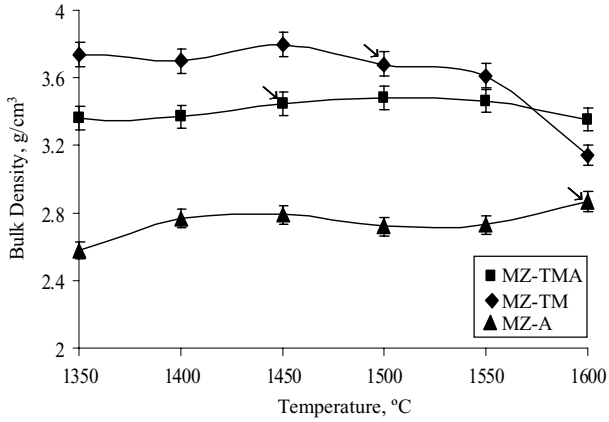

Figure 5 Bulk density of composites under various sintering conditions. Arrows indicate the temperature at which full mullite/ZrO_2 composites form.

Zircon disassociates to yield ZrO_2 and amorphous SiO_2 on heating. The amorphous SiO_2 softens with increasing temperature and starts to dissolve Al_2O_3 to form an amorphous aluminosilicate glass. Nucleation of mullite phase takes place after a critical alumina concentration is exceeded in the glass phase [33]. Additives such as CaO, MgO, TiO_2 were generally used to form a liquid (transient or permanent) phase in the sintering of zircon/alumina mixtures [8–10]. They can decrease the glass viscosity and retard the crystallization of the silicate phase [17]. It was reported that TiO_2 decreases the viscosity of silica by several orders of magnitude [34]. Enhanced transformation kinetics in TiO_2-doped diphasic mullite gels was attributed to the lowered glass viscosity due to TiO_2 doping [35]. Miranzo *et al.* [9] found that the reaction rate to form mullite/zirconia from the alumina/zircon mixture was significantly higher in the MgO-added compositions and this rate increased further with MgO content. In addition to the presence of additives, the seed particles significantly affect the mullite nucleation. It was found that the mullite transformation kinetics in aluminum borate doped-mullite was enhanced due to a similarity in the crystallographic structures, providing epitaxial nucleation sites for mullite [20].

It can be deduced based on Figs 2–4 that mullite and subsequently mullite/zirconia composite formation in MZ-TMA at lower temperatures can be attributed to the presence of both additives and templates in that additives lowered the glass viscosity providing a path for faster transport of species and isostructural aluminum borate templates served as heteroepitaxial sites for faster mullite nucleation and growth.

3.2. Densification

Fig. 5 shows the bulk density of composites as a function temperature. Note that the densities were not calculated based on the relative amounts of phases present at each temperature; rather, the density values measured by the Archimedes method were directly used. Arrows on the curves indicate the temperature at which the mullite/ZrO_2 composite fully forms. The composites have relatively constant densification, but at different levels, as a function of temperature. Template-free MZ-TM samples reached the highest bulk densities compared to the others except for at 1600°C. MZ-A samples did not densify until 1400°C and could only be sintered to a bulk density of 2.87 g/cm^3 even after sintering at 1600°C.

Sintering of mullite powders to densities close to the theoretical density generally requires high temperatures due to the low bulk and grain-boundary diffusion coefficients of mullite [9, 36]. Similarly, it is difficult to fabricate fully dense samples due to poor sinterability of the mixed zircon/alumina powders [37]. Therefore, modification of aluminosilicate phase with some additives was generally applied to enhance densification in the mullite-based composites [17]. This glass phase behaves as sintering aid and helps improve densification by means of viscous sintering [38]. Melo *et al.* [10] and Miranzo *et al.* [9] reported improved densification in an alumina/zircon mixture by adding TiO_2 and MgO, respectively. They attributed this effect to the formation of a transitory liquid phase at around 1400°C on TiO_2 addition and 1400–1425°C on MgO addition. Therefore, enhanced densification in MZ-TMA and MZ-TM can be attributed to the modification of aluminosilicate glass by TiO_2 and MgO. Poor sinterability of additive-free MZ-A samples necessitates that either hot pressing or higher temperatures and/or longer times are required to increase densification. Higher bulk density values in MZ-TM samples may be attributed to the density difference between the constituent oxides (e.g., ρ(aluminum borate) = 2.68 g/cm^3 (JCPDS # 32-0003)), ρ(mullite) = 3.17 g/cm^3, ρ(zircon) = 4.67 g/cm^3, ρ(alumina) = 3.99 g/cm^3, ρ(m-ZrO_2) = 5.83 g/cm^3 [39] and ρ(t-ZrO_2)=5.95 g/cm^3 (JCPDS # 17-0923)) and to the template-mullite reaction in MZ-TMA and MZ-A (e.g., a solid solution formation between aluminum borate and mullite [21]). More studies, however, are needed to explain the reactions between matrix powders, additives and

templates. Dedensification is observed after 1550°C in MZ-TM, which can be attributed to the random abnormal and/or anisotropic growth of the mullite grains.

From the densification (Fig. 5) and phase formation (Figs 2–4) results, it can be inferred that the reactions to form mullite and mullite/zirconia occur after the densification is complete because MZ-TMA and MZ-TM samples keep their respective bulk densities until full mullite/zirconia is attained.

3.3. Microstructure development

3.3.1. ZrO_2 evolution

SEM micrographs from the // samples are shown in Figs 6 and 7 for MZ-TMA and MZ-A samples, respectively.

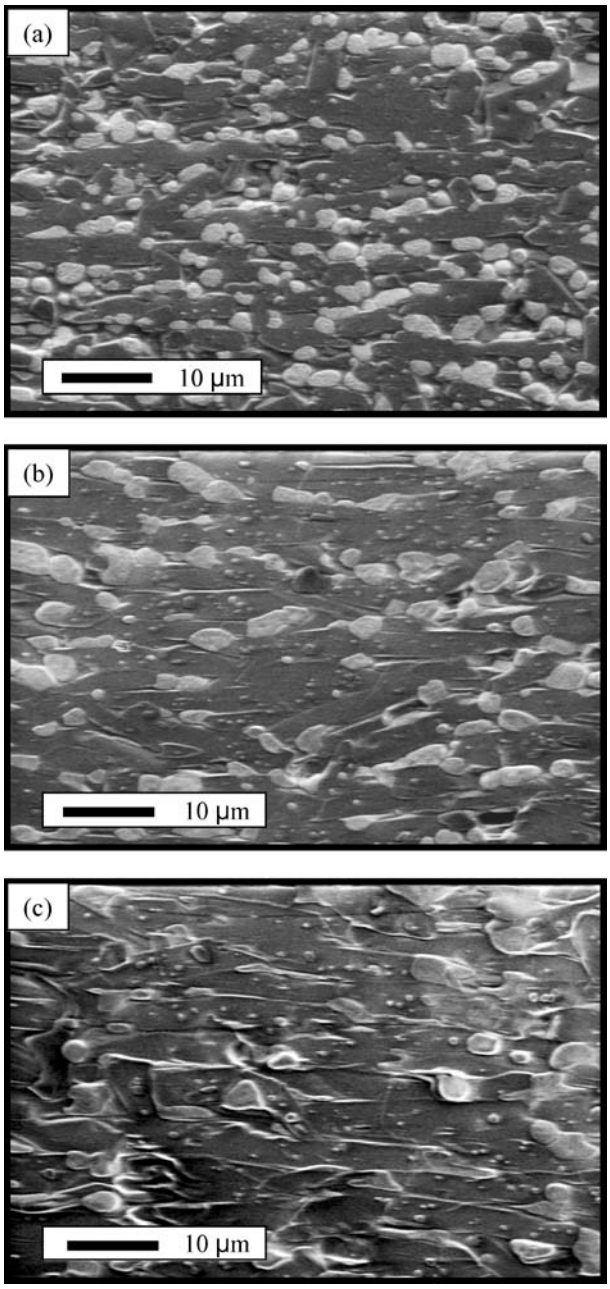

Figure 6 SEM pictures of the // MZ-TMA samples sintered at various temperatures for 2 h; (a) 1400°C, (b) 1550°C, and (c) 1600°C.

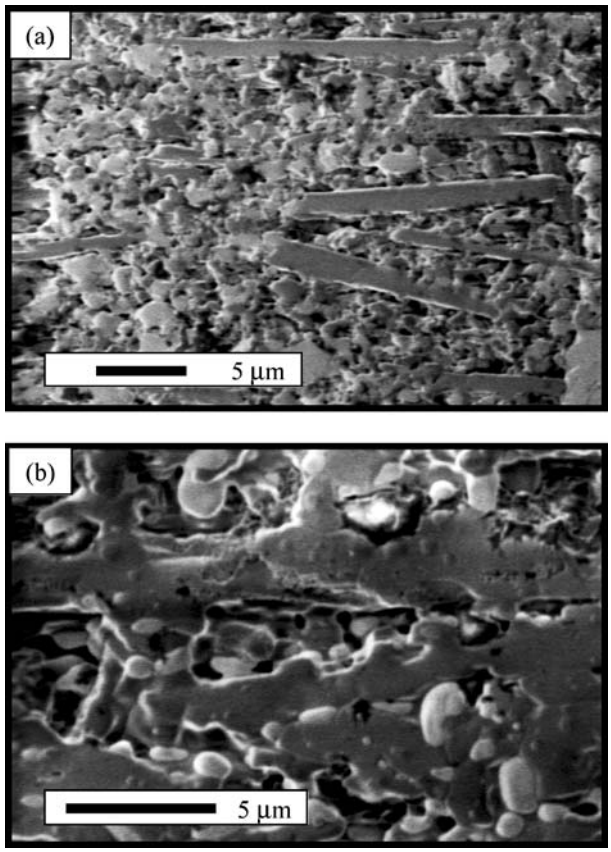

Figure 7 SEM pictures of the // MZ-A sintered at (a) 1450°C and (b) 1600°C for 2 h.

Microstructures of template-free MZ-TM sample are shown in Fig. 8. Because of the higher atomic number of zirconium, zirconia particles are seen brighter in the SEM. Figs 6–8 show that the zirconia grains are distributed throughout the darker mullite matrix. Two types of zirconia grains are present; one is intergranular ZrO_2 located between the mullite grains and the other one is intragranular ZrO_2 located inside the mullite grains. This is a generally observed microstructure development in the reaction sintering of zircon/alumina mixture [8–10, 13, 17]. In the MZ-TMA and MZ-TM samples (Figs 6 and 8), the intragranular ZrO_2 grains are small and spherical compared to the intergranular ZrO_2 grains having quasi-cubic or space-filling geometry at the triple junctions or angular shapes due to the constraint of the mullite grains. In the MZ-A samples (Fig. 7), however, there are rarely intragranular ZrO_2 present and almost all intergranular ZrO_2 grains are spherical.

Fig. 9 shows the *t*-ZrO_2 amount as a function of composition and temperature. For calculations, XRD patterns from as-sintered surfaces were used to avoid mechanical stress (e.g., polishing or grinding)-induced tetragonal to monoclinic (*t* to *m*) transformation [40, 41]. Polishing effect on ZrO_2 is compared in Fig. 10 for the MZ-TMA samples sintered at 1550°C for 2 h. Comparison of the XRD patterns from the as-sintered (Fig. 10a) and polished (Fig. 10b) surfaces indicate that no *t*-ZrO_2 is present in

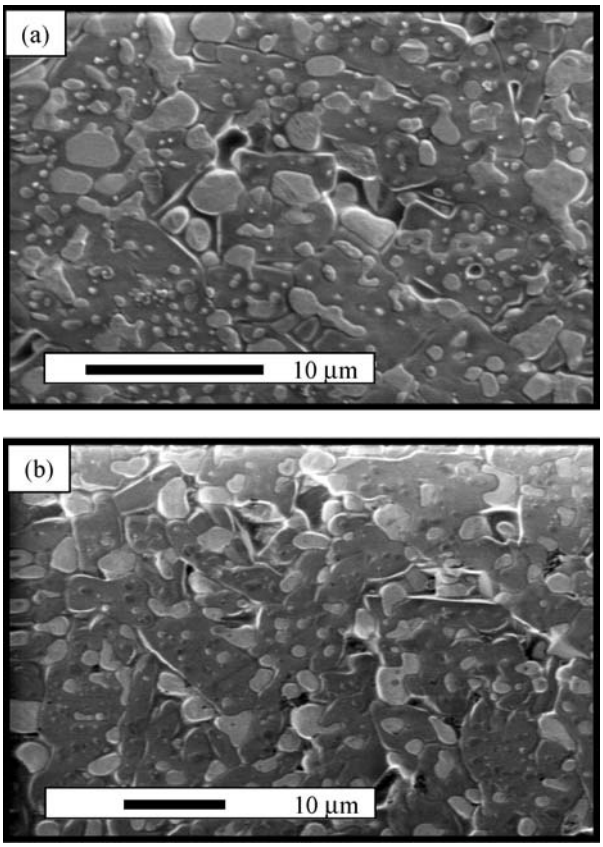

Figure 8 SEM pictures of the MZ-TM samples sintered at (a) 1450°C and (b) 1550°C for 2 h.

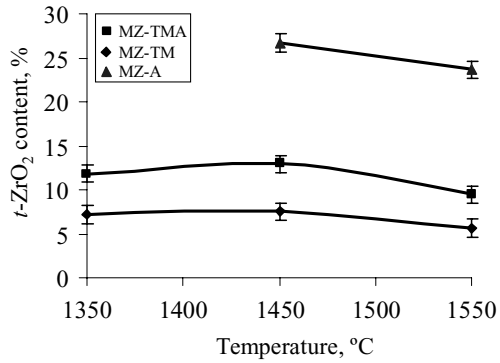

Figure 9 t- ZrO_2 content as a function of sintering temperature and composition.

the latter. Note that the presence of ZrO_2 is not dependent on the sample cutting direction (e.g., ⊥ or //). The *t*-ZrO_2 content was determined from the ratio of integrated XRD peak intensities of *t*-ZrO_2 (111) at $2\theta = 30.17°$ (JCPDS # 17-0923) to *m*-ZrO_2 ($\bar{1}11$) at $2\theta = 28.17°$ and *m*-ZrO_2 (111) at $2\theta = 31.46°$ (JCPDS # 37-1484), using the Garvie and Nicholson equation [42]. Note that the calculated *t*-ZrO_2 contents are with respect to the total ZrO_2 content in the composites, according to Equation 3. The MZ-A samples have more *t*-ZrO_2 content than the others at all temperatures.

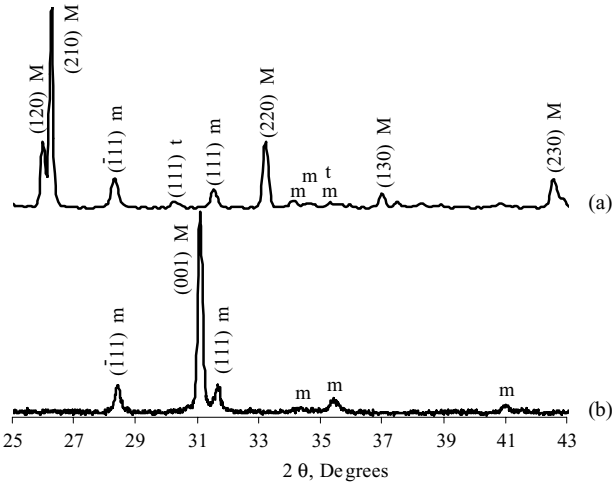

Figure 10 Comparison of XRD patterns of (a) // (sintered surface) and (b) ⊥-cut (polished surface) MZ-TMA samples sintered at 1550°C for 2 h. M: Mullite, m: monoclinic zirconia and t: tetragonal zirconia.

Stabilization of *t*-ZrO_2 can be accomplished by doping with such stabilizers as MgO, Y_2O_3, and CeO. Moreover, control of ZrO_2 grain size (either stabilized or not) can affect the stabilization of the tetragonal phase [43]. It was reported that *t*-ZrO_2 can be fully retained grain sizes up to 8 μm in 12Ce (12 mol.% ceria)-TZP and <1 μm in 2Y (2 mol.% yttria) -TZP [44]. Kyaw *et al.* [43] attributed the retention of 30% *t*-ZrO_2 to the finer ZrO_2 grain size (0.29 μm) in mullite/unstabilized ZrO_2 composites. As shown in Fig. 9, the composites had various amounts of *t*-ZrO_2 as a function of temperature and composition. This variation may be attributed to the co-doping of MgO and TiO_2 because it was shown in sintering of alumina/zircon that TiO_2 addition caused ZrO_2 grains to be located mostly in intergranular positions (~6% *t*-ZrO_2 when ~2.8 wt.% TiO_2 was added) [10] compared to mostly smaller intragranular ZrO_2 grains in the presence of MgO (~50–70% *t*-ZrO_2 when ~1.7 wt.% MgO was added) [9]. In addition, SiO_2 was reported to inhibit conversion of *t*-ZrO_2 to *m*-ZrO_2 in the ZrO_2-SiO_2 system [45, 46]. Upon $ZrSiO_4$ dissociation, ZrO_2 particles were immersed in the amorphous SiO_2 matrix, which stabilized ZrO_2 as *t*-ZrO_2. However, when SiO_2 starts to react with alumina to form mullite, ZrO_2 stabilization in the amorphous matrix is lost, giving rise to *m*-ZrO_2 formation with increasing sintering temperature [33]. In other words, larger particle size encourages *t*-ZrO_2 to *m*-ZrO_2 transformation on cooling [33, 43].

Table II summarizes grain size distributions of intergranular and intragranular ZrO_2 in the MZ-TMA and MZ-A samples. Particle sizes given correspond to the equivalent spherical particle diameters calculated from the measured area of the ZrO_2 grains from the SEM pictures. Measured area was corrected using Fullman relation [47]. The intragranular ZrO_2 grains are smaller than the intergranular ones in both MZ-TMA and MZ-A. In addition, grain size increases with temperature in MZ-TMA. A distinguishing difference between MZ-TMA and MZ-A

TABLE II Grain size distributions of intergranular and intragranular ZrO_2 in the MZ-TMA and MZ-A samples.

		Intragranular ZrO_2 (μm)				Intergranular ZrO_2 (μm)			
		Size finer than				Size finer than			
Sample code	Temp. (°C)	d_{10}	d_{50}	d_{90}	Mean size	d_{10}	d_{50}	d_{90}	Mean size
MZ-A	1600	0.12	0.27	0.46	0.38	0.40	0.80	1.36	0.95
MZ-TMA	1550	0.12	0.44	0.86	0.58	1.03	2.00	3.31	2.23
	1600	0.30	0.65	0.97	0.73	1.52	2.72	4.35	2.96

is that ZrO_2 grains are much bigger in the former, especially intergranular ZrO_2 grains. Intergranular ZrO_2 grains was reported to grow by Ostwald ripening [8, 48] and by grain boundary diffusion mechanisms [17] in which larger ZrO_2 grains grows at the expense of smaller ZrO_2 grains with increasing temperature. The presence of additives (or modification of glassy phase) highly facilitates the growth of intergranular ZrO_2 grains. The growth of intragranular ZrO_2, on the other hand, takes place by solid state diffusion via the mullite lattice [8], which is a more difficult and slower mechanism. Therefore, the intragranular ZrO_2 grains are much smaller compared to the intergranular ZrO_2 grains.

Although the MZ-A samples were poorly densified (Fig. 5), they have higher amount of t-ZrO_2 retained at room temperature (Fig. 9). Retention of more t-ZrO_2 at a less dense structure can be partly attributed to finer ZrO_2 grain size (Table II). Porous structure effectively decreases the growth rate of ZrO_2 particles by increasing the diffusion distance, which results in finer ZrO_2 grain size, promoting t-ZrO_2 retention [33]. In addition, porous structure reduces compaction tension on ZrO_2 grains, which facilitates t-ZrO_2 to m-ZrO_2 transformation because the ZrO_2 grains in a dense body are subjected to a larger strain energy due to constraint of the mullite matrix compared to those in a less dense body [43, 49]. In other words, the t-ZrO_2 to m-ZrO_2 transformation is martensitic with a 3–5% volume expansion on cooling and if the mullite matrix prevents this volume change on ZrO_2, the transformation can be delayed and, furthermore, t-ZrO_2 can be retained at room temperature [50]. Apparently, the constraint of mullite matrix to prevent ZrO_2 grain shape during cooling is lost or weakened in the porous structures, giving rise to more m-ZrO_2 formation in MZ-A. In the dense MZ-TMA samples, however, more t-ZrO_2 is expected due to more compaction tension of mullite on ZrO_2. As seen from Table II, however, ZrO_2 grain size is much bigger, as compared to MZ-A, due to the presence of additives, contributing to m-ZrO_2 formation. Dense MZ-TM samples have lower t-ZrO_2 content than MZ-TMA, which can be attributed to the lack of template particles because the isostructural templates induce accelerated mullite formation (Fig. 4) and, thus, more amount of smaller intragranular ZrO_2 particles are entrapped by growing mullite grains. Based on these results, it can be inferred that compaction tension (or density) and ZrO_2 grain size are the controlling factors for t-ZrO_2 content retained at room temperature.

3.3.2. Texture evolution in mullite

Fig 6 and 7 show morphological texture development for the // MZ-TMA and MZ-A samples, respectively. Texture development in MZ-TMA (Fig. 6) improves very fast with increasing temperature, resulting in highly morphologically textured mullite grains. In MZ-A, however, almost no growth of templates takes place at 1450°C (Fig. 7a) and elongated grains with rather rough surfaces are obtained at 1600°C (Fig. 7b). Crystallographic texture evolution for mullite in the ⊥-cut MZ-TMA and MZ-A samples is evaluated from Figs 2 and 3, respectively. Absence of aluminum borate (*hk0*) and (*hkl*) peaks and presence of only (*00l*) peaks indicate an evidence of good template orientation in [001] during tape casting. Preferential growth of mullite depends on the initial orientation of templates during the green body processing. Both graphs indicate that once mullite forms, its orientation is always (*00l*), proving that aluminum borate templates serve as sites for both mullite formation and grain orientation in [001] because mullite peaks other than (*00l*) does not appear in the XRD patterns. Only in the MZ-A does the main peaks of mullite appear at $T \geq 1550$°C (Fig. 3). These weak mullite peaks can be attributed to the mullite nucleated in the matrix, that is, independent of templates. Fig. 10 indicates further evidence of mullite texture. Comparison of the XRD patterns obtained from the // and ⊥-cut samples (see Fig. 1 for sample configuration) clearly prove strong mullite texture in [001] because only (*hk0*) peaks in the // sample and only (00l) peaks in the ⊥-cut sample are present. Note that (*hkl*) peaks (e.g., (111) at $2\theta = 35.27°$ and (121) at $2\theta = 40.87°$) do not appear in both patterns, which is an indicative of strong fiber texture in mullite.

The texture fraction (f) of mullite in the mullite/zirconia composites was calculated using Equation 1. Fig. 2 indicates that when mullite forms, its orientation is (*00l*) and, therefore, f is ~1 for MZ-TMA. As for MZ-A (Fig. 3), however, main mullite peaks appear in addition to the (*00l*) peaks. f is calculated to be 0.93 for samples sintered at 1600°C for 2 h. Although the Lotgering factor is an easy method to calculate texture fraction, it does not give information about the texture distribution around [001]. Therefore, the texture distribution around [001] can be quantitatively determined from the rocking curves. For each sample, orientation distribution curves were obtained by fitting the corrected rocking curve data to Equation 2, and then the orientation distribution parameter r for mullite was calculated. Fig. 11 shows orientation distribution curves of mullite in the MZ-A and MZ-TMA samples

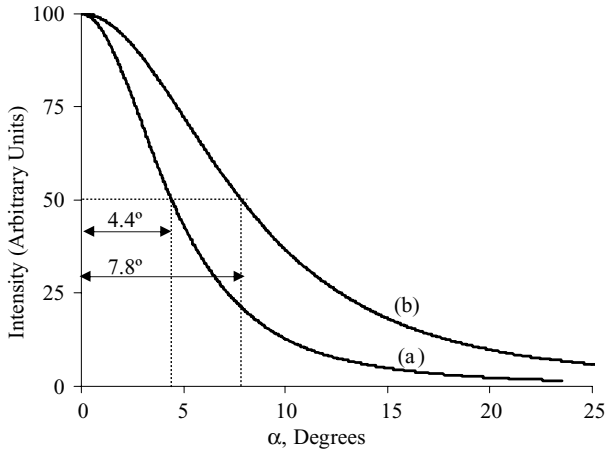

Figure 11 Orientation distribution curves for (a) MZ-TMA sintered at 1450°C and (b) MZ-A sintered at 1600°C for 2 h. Values on the graph show the angle at half width at half maximum (HWHM).

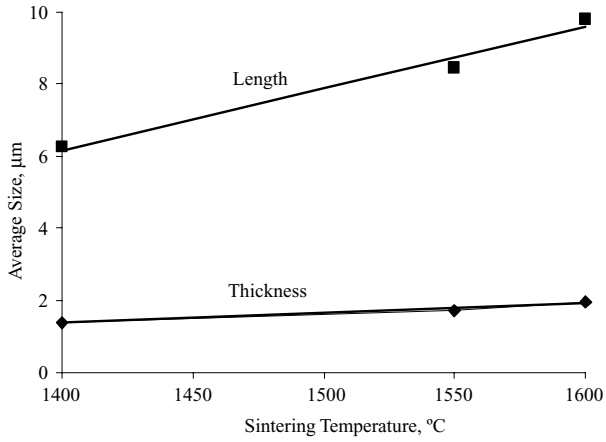

Figure 12 Growth of mullite grains in the length and thickness directions as a function of sintering temperature (for 2 h) in the MZ-TMA samples.

after mullite formation is complete in each case. For MZ-A and MZ-TMA, r was calculated to be 0.31 and 0.22, respectively. The curves indicate that the elongated mullite grains are oriented within 15.6° (i.e., half width at half maximum (HWHM) is 7.8°) in MZ-A and 8.8° (i.e., HWHM is 4.4°) in MZ-TMA around [001]. Higher r in the MZ-A can be attributed to the mullite formation in the matrix, that is, mullite nucleated independent of the templates, which increases randomness. Increase in the r parameter corresponds to a broadening of the orientation distribution in [001] because the r parameter is closely related to the width of the texture distribution of the anisotropic mullite grains.

The liquid (or glass) in the system promotes the growth of aligned template particles (or elongated mullite grains after mullite formation), which is characterized by nucleation or reprecipitation of mullite on the bigger (or lower surface area) template particles. This process results in the anisotropic growth of mullite grains, which stresses that the aspect ratio of the template particles must be high and the matrix grain size must be as fine as possible at the time of densification. Fig. 12 shows mullite grain growth in the length and thickness directions as a function of temperature in the MZ-TMA samples. (001) growth of mullite grains reveals that the growth in the length direction is faster than the thickness direction because the activation energies for the grain length and thickness directions were calculated to be 690 kJ/mol and 790 kJ/mol in the textured, 5 wt% TiO_2 doped-mullite, respectively [35]. It was determined that mullite tends to have acicular shapes under unconstrained growth conditions such as directional solidification and vapor-solid synthesis where the acicular particles grew in the c-axis and were bounded by $\{110\}$ or $\{111\}$ surfaces [51, 52]. These results indicate that $\{110\}$ and $\{111\}$ planes have a lower energy than the other planes, giving rise to the growth of elongated grains in [001]. Such a growth habit is strongly related to the crystal structure of mullite because it is composed of octahedral AlO_6 chains aligned in the c-direction and cross-linked by corner-shared AlO_4 and SiO_4 tetrahedra [53].

Fig. 8 depicts that the mullite grains are mostly anisotropic and randomly-oriented as well as some of them are small and equiaxed in the MZ-TM samples. Mullite grains in the MZ-TMA samples (Fig. 6), however, were evenly regulated in the direction of initial template particles' orientation, which indicates that random anisotropic grain growth in mullite was successfully prevented by the templates and that a template content of 10 wt% was adequate to control the microstructure, as also reflected by strong (00l) peaks in Fig. 2. Fig. 7 shows for the MZ-A samples that there seems to be not much of growth on the templates despite the fact that XRD shows a strong mullite texture in [001] together with weak mullite main ($hk0$) peaks after sintering at $T \geq 1550$°C (Fig. 3). A high crystallographic texture in spite of a poor microstructural texture reveals that the mullite grains adjacent to the template particles might have the same crystallographic orientation as the templates because mullite growth occurs by nucleation on the template particles. However, this needs to be verified by orientation image microscopy or transmission electron microscopy. Similar results were also observed in TGG of mullite textured with acicular mullite templates [22].

As mentioned before, the aim of this study is to fabricate mullite/zirconia ceramic composites with highly textured mullite in [001] as well as homogeneously dispersed t-ZrO_2 grains (rather than m-ZrO_2 from the transformation toughening and microcracking points of views). In the MZ-TMA samples sintered at 1450°C for 2 h, 100% mullite texture and ~13% t-ZrO_2 in the final mullite/zirconia composite were obtained. Higher amount of t-ZrO_2 (~24%) was retained in the MZ-A samples sintered at 1550°C, but densification was limited and low. Because a high modulus of the mullite matrix and small ZrO_2 grain size (typically <1 μm) are effective in suppressing martensitic t-ZrO_2 to m-ZrO_2 transformation [50], increasing the amount of initial template content (up to

as high as 25 wt.%) can confine ZrO_2 grains between the growing template particles or mullite grains such that little room will be available for the growth of ZrO_2 grains because of the smaller intertemplate spacing. Another possible solution is to utilize Y_2O_3 as a stabilizing agent to retain *t*-ZrO_2 at room temperature [48]. These processing approaches as well as mechanical properties of resulting composites will be reported later.

4. Conclusions

Dense mullite/zirconia composites were successfully fabricated by reactive sintering of alumina and zircon powders. Acicular aluminum borate templates (10 wt%) served as heteroepitaxial sites for mullite nucleation and growth in [001] in the composites. Additives TiO_2 and MgO modified the aluminosilicate glass by decreasing its viscosity and promoted liquid phase sintering, resulting in faster transport of species. Therefore, mullite/zirconia composites were fully obtained at 1450°C for the samples containing both templates and additives, as compared to 1500°C for the samples containing only additives and to 1600°C for the samples containing only templates. In addition, SiO_2 remained amorphous during the reactions.

Mullite/zirconia phase formation occurred after the matrix densification was complete. Texture development also started after the matrix densification. Mullite/zirconia composites with highly textured mullite (Lotgering factor for mullite ∼1) were fabricated at 1450°C in the presence of both additives and templates. A high quality of mullite texture with a degree of orientation parameter of 0.22 and a very narrow distribution of elongated mullite grains within 8.8° around [001] were obtained in the composites. Nearly 13% tetragonal ZrO_2 in the final mullite/zirconia composite was retained in the presence of additives and templates. Higher amount of tetragonal ZrO_2 (∼24%) was retained in the presence of only templates, but densification was limited and very low even after sintering at 1550°C. Compaction tension (or density) and ZrO_2 grain size were found to be the factors controlling *t*-ZrO_2 content retained at room temperature.

Acknowledgments

The financial support of Gebze Institute of Technology (Project #`s 02-B-03-01-13 and 02-A-03-01-10) is greatly appreciated. Authors would like to thank Shikoku Chemical Co. (Japan) for supplying aluminum borate whiskers and Mr. Adem Şen for XRD studies.

References

1. T. I. MAH and K. S. MAZDIYASNI, *J. Am. Ceram. Soc.* **66** (1983) 699.
2. I. A. AKSAY, D. M. DABBS and M. SARIKAYA, *ibid.* **74** (1991) 2343.
3. R. TORRECILLAS, G. FANTOZZI, S. DE AZA and J. S. MOYA, *Acta Mater.* **45** (1997) 897.
4. P. D. D. RODRIGO and P. BOCH, *Int. J. High Tech. Ceram.* **1** (1985) 3.
5. K. A. KHOR, L. G. YU, Y. LI, Z. L. DONG, Z. A. MUNIR, *Mat. Sci. Eng.* **A339** (2003) 286.
6. N. CLAUSSEN and J. JAHN, *J. Am. Ceram. Soc.* **63** (1980) 228.
7. P. BOCH and T. CHARTIER, *ibid.* **74** (1991) 2448.
8. P. PENA, P. MIRANZO, J. S. MOYA and S. DE AZA, *J. Mater. Sci.* **20** (1985) 2011.
9. P. MIRANZO, P. PENA, J. S. MOYA and S. DE AZA, *ibid.* **20** (1985) 2702.
10. M. F. MELO, J. S. MOYA, P. PENA and S. DE AZA, *ibid.* **20** (1985) 2711.
11. M. SEABAUGH, Ph. D. Thesis, The Pennsylvania State University (1998).
12. G. L. MESSING, E. M. SABOLSKY, S. TROLIER-MCKINSTRY, C. DURAN, S. KWON, B. BRAHMAROUTU, P. PARK, H. YILMAZ, P. W. REHRIG, K. B. EITEL, E. SUVACI and M. SEABAUGH, *Criti. Rev. Solid State Mater. Sci.* **29** (2004) 45.
13. P. DESCAMPS, S. SAKAGUCHI, M. POORTEMAN and F. CAMBIER, *J. Am. Ceram. Soc.* **74** (1991) 2476.
14. F. CAMBIER, C. BAUDIN, P. PILATE and A. LERICHE, *Br. Ceram. Trans.* **83** (1984) 196.
15. T. KOYAMA, S. HAYASHI, A. YASUMORI, K. OKADA, M. SCHMUCKER and H. SCHNEIDER, *J. Eur. Cer. Soc.* **16** (1996) 231.
16. J. M. WU and C. M. LIN, *J. Mater. Sci.* **26** (1991) 4631.
17. Y.-J. LIN, *J. Mater. Res.* **14** (1999) 916.
18. M. IHARA, K. IMAI, J. FUKUNAGA and N. YOSHIDA, *J. Ceram. Soc. Jpn.* **78** (1980) 1014
19. J. YLA-JAASKI and H.-U. NISSEN, *Phys. Chem. Minerals.* **10** (1983) 47.
20. S.-H. HONG and G. L. MESSING, *J. Am. Ceram. Soc.* **80** (1997) 1551.
21. I. E. GONENLI and G. L. MESSING, *J. Eur. Cer. Soc.* **21** (2001) 2495.
22. S.-H. HONG and G. L. MESSING, *J. Am. Ceram. Soc.* **82** (1999) 867.
23. Y. HIRATA, S. MATSUSHITA, Y. ISHIHARA and H. KATSUKI, *J. Am. Ceram. Soc.* **74** (1991) 2438.
24. C. NISCHIK, M. M. SEIBOLD, N. A. TRAVITZKY and N. CLAUSSEN, *ibid.* **74** (1991) 2464.
25. C. DURAN and Y. K. TUR, *Mater. Lett.* **59** (2005) 245.
26. F. K. LOTGERING, *J. Inorg. Nucl. Chem.* **9** (1959) 113.
27. M. M. SEABAUGH, M. D. VAUDIN, J. P. CLINE, and G. L. MESSING, *J. Am. Ceram. Soc.* **83** (2000) 2049.
28. M. D. VAUDIN, "TexturePlus", National Inst. of Std. and Tech., Ceramics Division, Gaithersburg, MD, USA.
29. A. MARCH, *Z. Kristallogr.* **81** (1932) 285.
30. W. A. DOLLASE, *J. Appl. Cryst.* **19** (1986) 267.
31. M. D. SACKS, Y.-J. LIN, G. W. SCHEIFFELE, K. WANG and N. BOZKURT, *J. Am. Ceram. Soc.* **78** (1995) 2897.
32. J. C. HULING and G. L. MESSING, *ibid.* **74** (1991) 2374.
33. S.-K. ZHAO, Y. HUANG, C.-A. WANG, X.-X. HUANG and J.-K. GUO, *Mater. Lett.* **57** (2003) 1716.
34. N. P. BANSAL and R. H. DOREMUS, "Handbook of Glass Properties" (Academic Press, New York, 1986)
35. S.-H. HONG and G. L. MESSING, *J. Am. Cream. Soc.* **81** (1998) 1269.
36. K. A. KHOR and Y. LI, *Mat. Sci. and Eng.* **A256** (1998) 271.
37. S.-K. ZHAO, Y. HUANG, C.-A. WANG, X.-X. HUANG and J.-K. GUO, *Ceram. Int.* **29** (2003) 49.
38. S. K. ZHAO, X. X. HUANG and J. K. GUO, *J. Mater. Sci. Lett.* **19** (2000) 707.
39. "Handbook of Chemistry and Physics" (CRC Press, Boca Raton, FL, USA, **E53**, 1985/1986) 66th edn.
40. N.-L. WU, T.-F. WU and I. A. RUSAKOVA, *J. Mater. Res.* **16** (2001) 666.
41. V. YAROSHENKO and D. S. WILKINSON, *J. Am. Ceram. Soc.* **84** (2001) 850.
42. R. C. GARVIE and P. S. NICHOLSON, *ibid.* **55** (1972) 303.
43. T. M. KYAW, Y. OKAMOTO and K. HAYASHI, *J. Mat. Sci.* **32** (1997) 5497.

44. P. F. BECHER and M. V. SWAIN, *J. Am. Ceram. Soc.* **75** (1992) 493.
45. V. S. NAGARAJAN and K. J. RAO, *J. Mater. Sci.* **24** (1989) 2140.
46. S. W. WANG, X. X. HUANG and J. K. GUO, *ibid.* **32** (1997) 197.
47. R. L. FULLMAN, *J. Metals.* (1953) 447.
48. K. DAS, B. MUKHERJEE and G. BANERJEE, *J. Eur. Ceram Soc.* **18** (1998) 1771.
49. T. EBADZADEH and E. GHASEMI, *Mat. Sci. Eng.* **A283** (2000) 289.
50. S. YANGYUN and R. J. BROOK, *Sci. Sinter.* **17** (1985) 35.
51. D. MICHEL, L. MAZEROLLES and R. PORTIER, *Ceram. Trans.* **6** (1990) 435.
52. K. OKADA and N. OTUSKA, *J. Am. Ceram. Soc.* **74** (1991) 2414.
53. J. YLA-JAASKI and H.-U. NISSEN, *Phys. Chem. Miner.* **10** (1983) 47.

Received 16 January 2004
and accepted 7 July 2005